Supporting Information

Hot-substrate deposition of all-inorganic perovskite films for low-temperature processed high-efficiency solar cells†

Ze Wang,[a] Xiaodong Liu,*[ab] Yiwei Lin,[a] Yingjie Liao,[a] Qi Wei,[d] Haoran Chen,[c] Jingjing Qiu,[c] Yonghua Chen*[cd] and Yonghao Zheng*[abe]

[a]School of Optoelectronic Science and Engineering, University of Electronic Science and Technology of China (UESTC), Chengdu 610054, China

[b]Center for Applied Chemistry, University of Electronic Science and Technology of China (UESTC), Chengdu 611731, China

[c]Key Laboratory of Flexible Electronics (KLOFE) & Institution of Advanced Materials (IAM), Jiangsu National Synergetic Innovation Center for Advanced Materials (SICAM), Nanjing Tech University (NJTECH), Nanjing 211816, Jiangsu, China

[d]Shaanxi Institute of Flexible Electronics (SIFE), Northwestern Polytechnical University (NPU), 127 West Youyi Road, Xi'an 710072, China

[e]Jiangsu Key Laboratory for Carbon-Based Functional Materials & Devices, Soochow University, Suzhou 215123, China

* Corresponding authors:

E-mail: xdliu@uestc.edu.cn, iamyhchen@njtech.edu.cn, zhengyonghao@uestc.edu.cn

Contents

1. **Photo image of hot plate mounted spin-coater** **S3**
2. **Photographs of $CsPbI_2Br$ films** **S4**
3. **Formation processes of cubic phase $CsPbI_2Br$ films** **S5**
4. **Photophysical characteristics of the $CsPbI_2Br$ films** **S7**
5. **Large scale SEM images of the $CsPbI_2Br$ films** **S9**
6. **AFM height images of the $CsPbI_2Br$ films** **S10**
7. **Thermal stability of the $CsPbI_2Br$ film tested in glove box** **S11**
8. **Optimization of substrate temperatures** **S12**
9. **Optimization of post-annealing temperatures** **S15**
10. ***J-V* curves measured under different scan rates** **S19**
11. ***J-V* curves measured under different scan directions** **S20**
12. **Thermal stability tests of $CsPbI_2Br$ and $CH_3NH_3PbI_3$ PSCs** **S21**
13. **References** **S22**

1. Photo image of hot plate mounted spin-coater

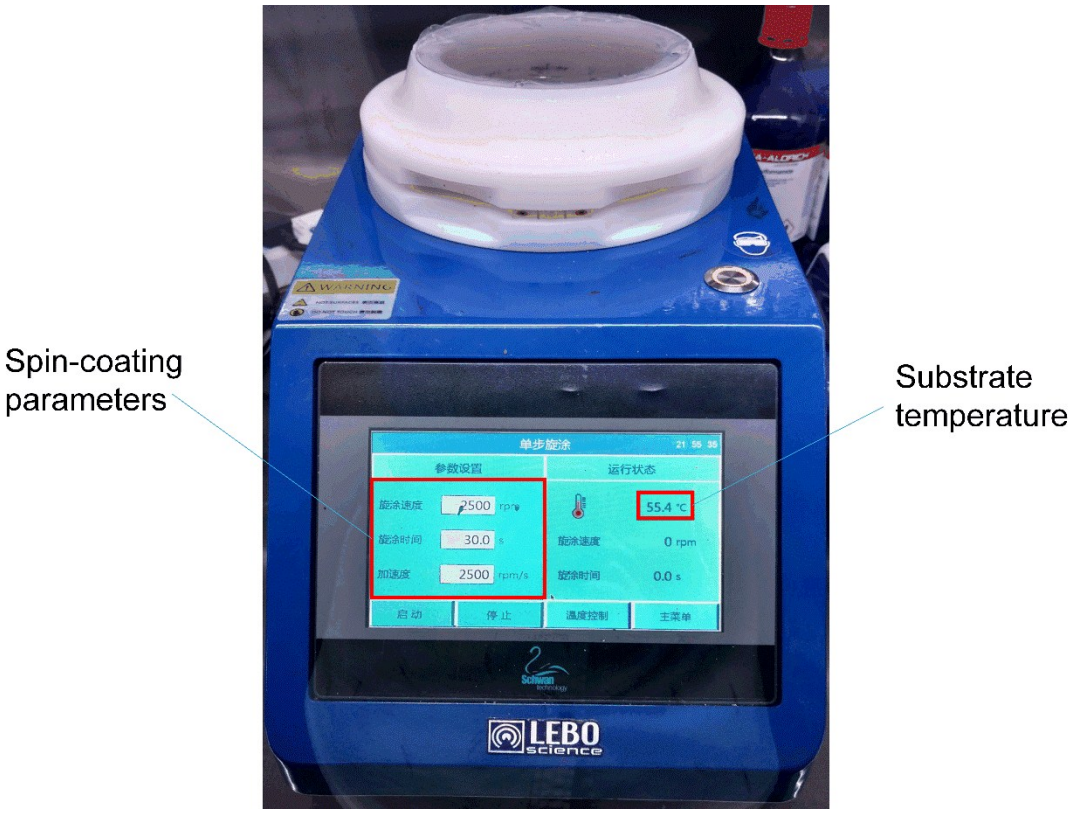

Fig. S1 Real photo of hot plate mounted spin-coater used in this work.

In this work, a specially designed spin-coater with a mounted hot plate (in other word, our spin-coater has the heating function) was used to achieve precise control of substrate temperature. The SnO_2-coated ITO substrate was placed on the spin-coater, and then heated to the desired temperature (e.g., 55 °C) using the hot plate integrated into the spin-coater. During the spin-coating process, the substrate was continuously heated on the hot plate at 55 °C, which maintains the 55 °C substrate temperature.

2. Photographs of $CsPbI_2Br$ films

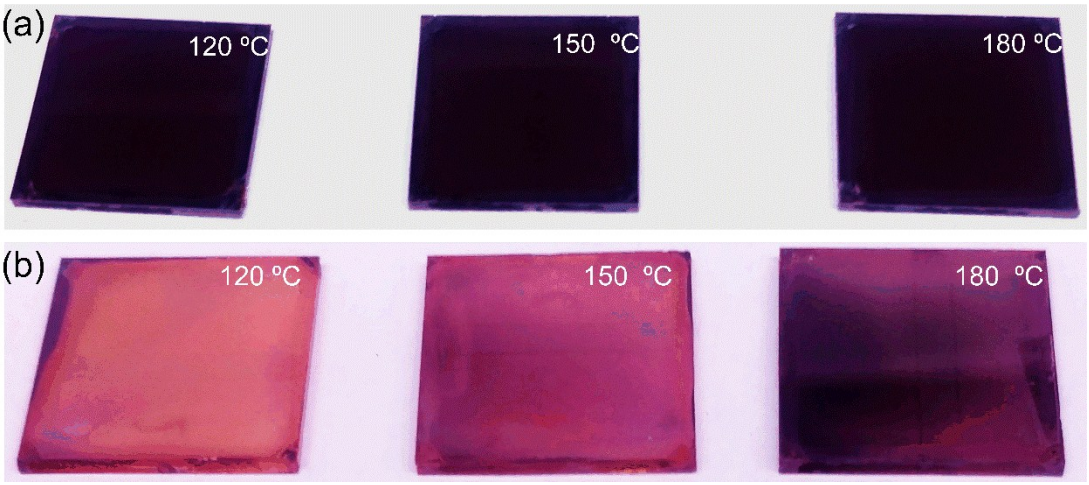

Fig. S2 Photographs of $CsPbI_2Br$ films prepared by (a) hot-casting (substrate temperature was kept at 55 °C) and (b) RT-casting methods with different post-annealing temperatures.

Hot-casting processed $CsPbI_2Br$ films presented a dark brown color, almost independent on the post-annealing temperature (120-180 ºC). In contrast, RT-casting processed $CsPbI_2Br$ films exhibited an orange yellow at a low post-annealing temperature of 120 ºC, and the color turned to partially black upon post-annealing at 180 °C. This indicates that hot-casting processed $CsPbI_2Br$ films are beneficial for cubic phase formation at a low post-annealing temperature compared to RT-casting processed $CsPbI_2Br$ films.

3. Formation processes of cubic phase $CsPbI_2Br$ films

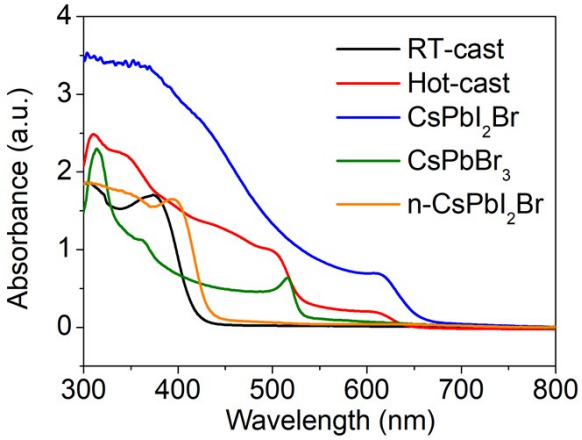

Fig. S3 UV-vis absorption of the perovskite precursor films prepared by RT-casting and hot-casting methods. The absorption spectra of $CsPbI_2Br$, $CsPbBr_3$ and non-perovskite $CsPbI_2Br$ (n-$CsPbI_2Br$) were plotted together in Fig. S3.

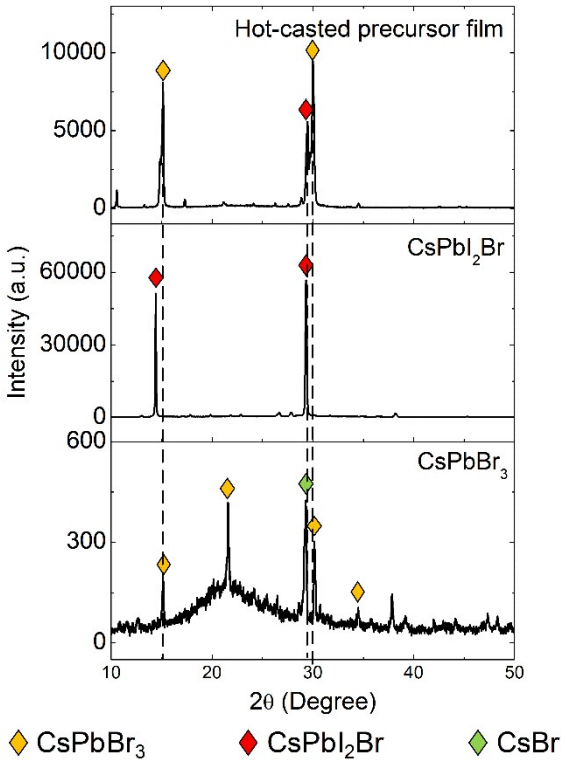

Fig. S4 XRD patterns of $CsPbBr_3$, $CsPbI_2Br$ and hot-casted precursor films.

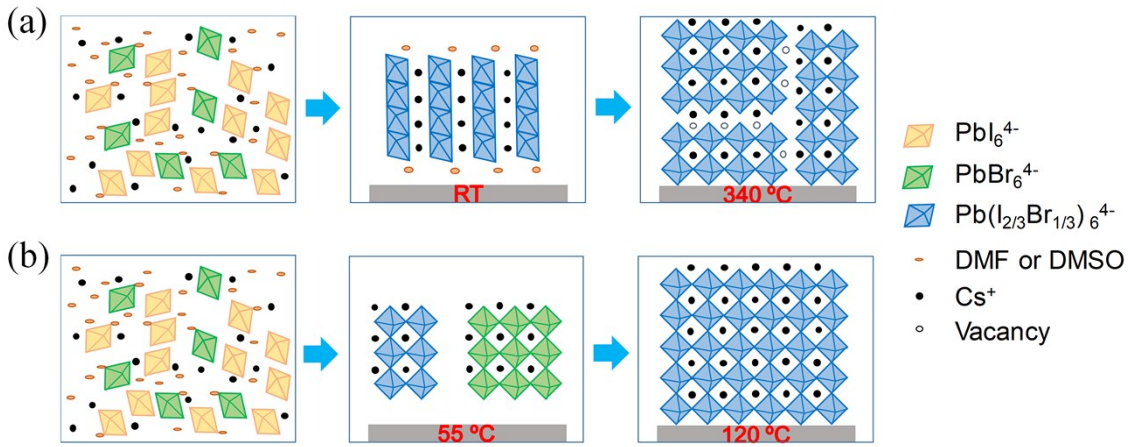

Fig. S5 Scheme for the formation of the $CsPbI_2Br$ perovskite films via the (a) RT-casting and (b) hot-casting processes.

4. Photophysical characteristics of the $CsPbI_2Br$ films

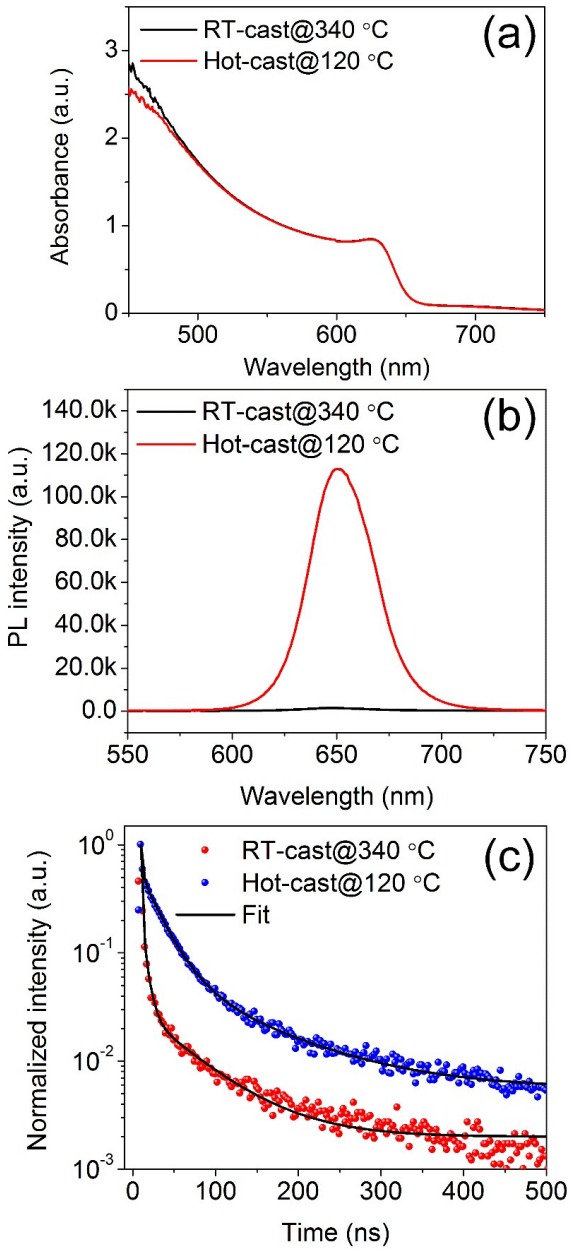

Fig. S6 (a) UV-vis absorption, (b) PL and (c) TRPL spectra of $CsPbI_2Br$ films fabricated by conventional RT-casting and hot-casting methods.

Table S1. PL lifetimes extracted from TRPL spectra for $CsPbI_2Br$ films prepared by the two different methods.

Method	A_1	$\tau_1{}^a$ (ns)	A_2	$\tau_2{}^a$ (ns)	A_3	$\tau_3{}^a$ (ns)	τ_{ave} (ns)
RT-casting	0.0016	63.13	0.0164	6.16	0.9820	0.03	0.23
Hot-casting	0.1932	23.01	0.0265	103.61	0.7823	0.51	7.59

[a]The TRPL decay curves were fitted using a tri-exponential decay function:

$$y = y_0 + A_1 e^{-(x-x_0)/\tau_1} + A_2 e^{-(x-x_0)/\tau_2} + A_3 e^{-(x-x_0)/\tau_3}$$

where A_1, A_2 and A_3 are the relative amplitudes of the components, the lifetime of τ_1 is associated with defect trapping recombination, and τ_2 and τ_3 are both associated with free carrier radiative recombination.[1,2]

5. Large scale SEM images of the $CsPbI_2Br$ films

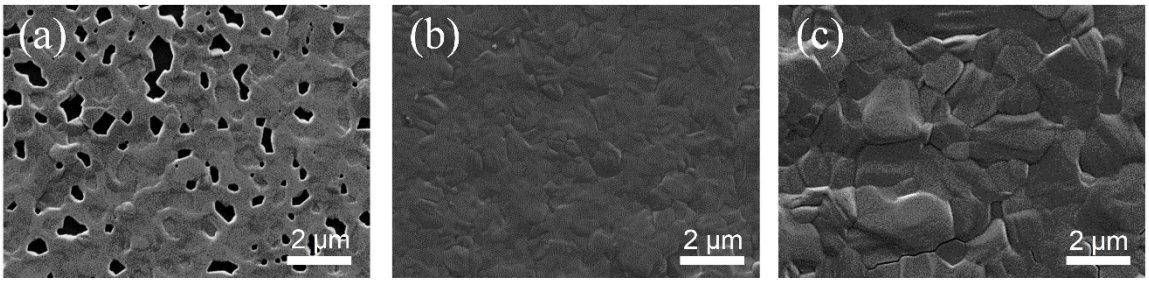

Fig. S7 Large scale SEM images of $CsPbI_2Br$ films prepared from the different methods: (a) conventional RT-casting process with subsequent post-annealing at 340 °C; hot-casting process with subsequent post-annealing at (b) 120 °C and (c) 180 °C.

With increasing the post-annealing temperature of the hot-casted precursor film from 120 °C to 180 °C, the grain size of perovskite increases. It is well known that the perovskite crystal growth rate is highly related to the solvent evaporation rate.[3] High post-annealing temperature results in the rapid volatilization of DMSO/DMF, and therefore the rapid perovskite crystal growth from a few nucleation sites, leading to the formation of large grains; low temperature results in the low solvent evaporating rate, which allows the crystal growth from a large number of nucleation sites, leading to the formation of small grains.[4,5]

6. AFM height images of the $CsPbI_2Br$ films

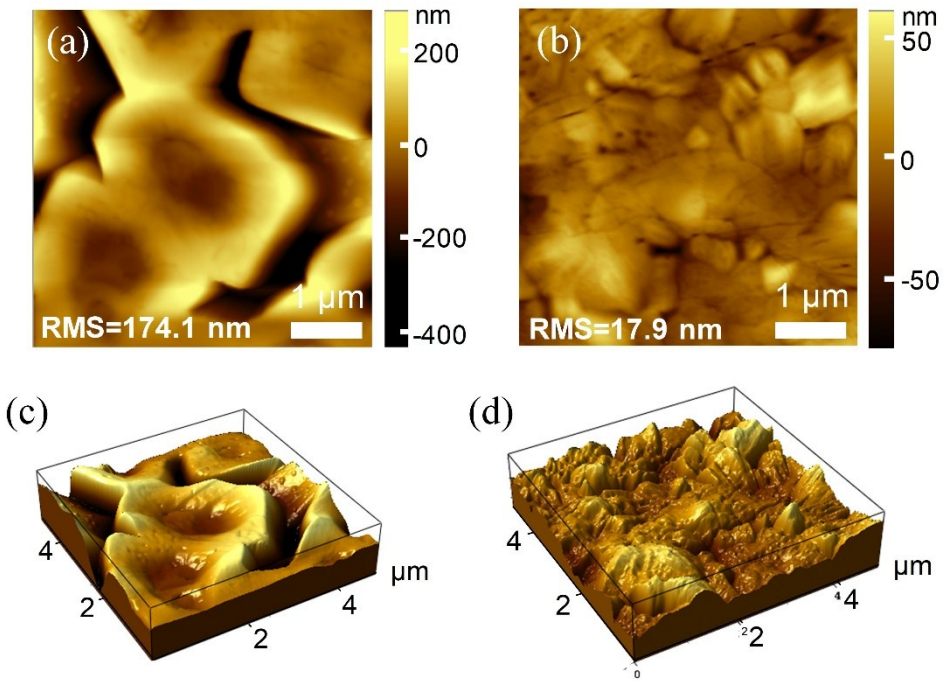

Fig. S8 (a,b) 2D AFM height images and (c,d) corresponding 3D images (5 μm × 5 μm) of $CsPbI_2Br$ films prepared from the different methods: (a,c) conventional RT-casting process with subsequent post-annealing at 340 °C; (b,d) hot-casting process with subsequent post-annealing at 180 °C.

7. Thermal stability of the $CsPbI_2Br$ film tested in glove box

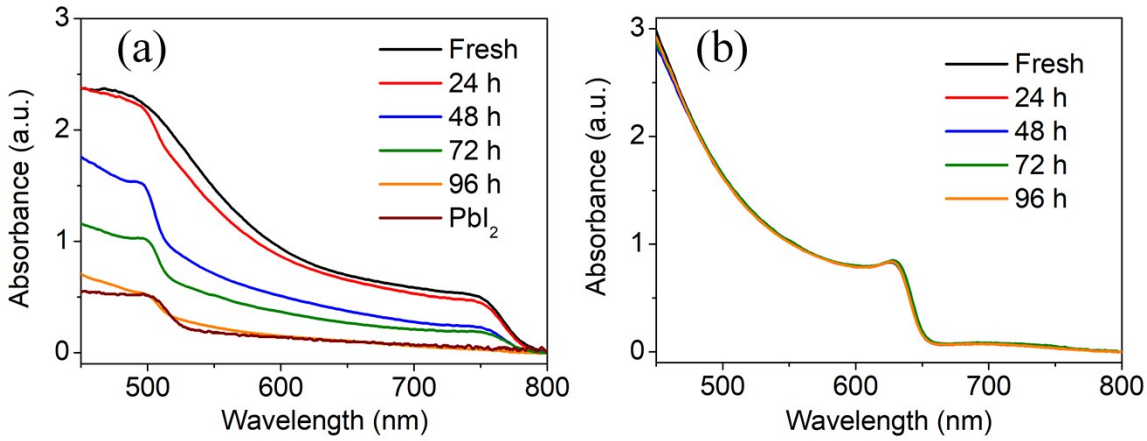

Fig. S9 Temporal evolution of UV-vis absorption spectra of (a) traditional organic-inorganic hybrid perovskite $CH_3NH_3PbI_3$ and (b) hot-casting processed $CsPbI_2Br$ films, which were placed on a hot plate at 100 °C in a N_2-filled glove box with H_2O and O_2 levels below 1 ppm.

8. Optimization of substrate temperatures

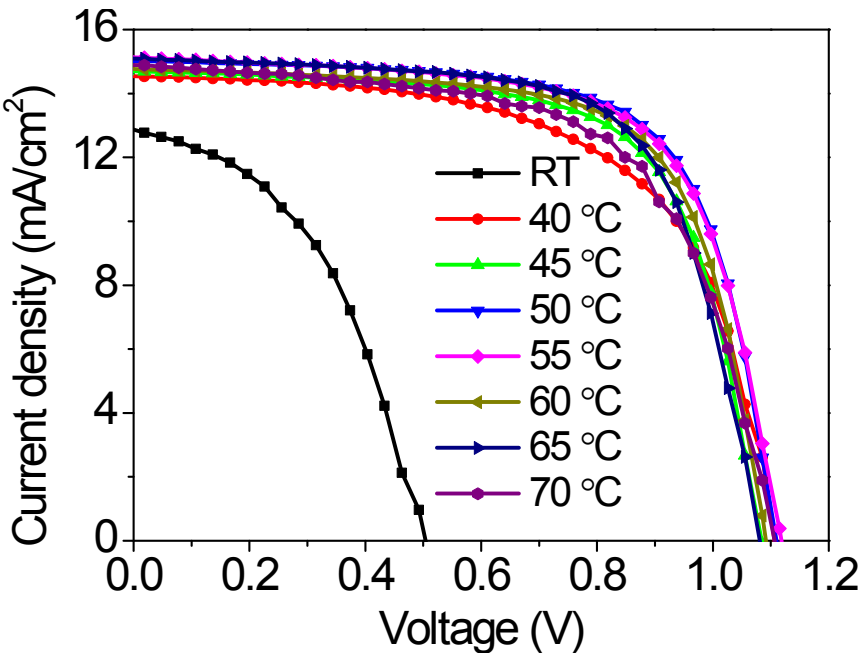

Fig. S10 *J-V* characteristics of $CsPbI_2Br$-based PSCs fabricated by RT-casing and hot-casting methods with different substrate temperatures. All the perovskite films underwent post-annealing at 340 °C for 10 min.

Table S2. Photovoltaic performance of the $CsPbI_2Br$-based PSCs fabricated by RT-casing and hot-casting methods with different substrate temperatures. All the perovskite films underwent post-annealing at 340 °C for 10 min.

Substrate temp. (°C)	V_{oc}[a] (V)	J_{sc}[a] (mA cm^{-2})	FF[a] (%)	PCE[a] (%)
RT	0.50 (0.50 ± 0.02)	12.85 (12.60 ± 0.64)	45.3 (43.8 ± 2.2)	2.91 (2.74 ± 0.13)
40	1.11 (1.12 ± 0.01)	14.54 (14.55 ± 0.24)	61.4 (59.2 ± 1.9)	9.91 (9.52 ± 0.38)
45	1.08 (1.09 ± 0.01)	14.69 (14.52 ± 0.28)	66.9 (66.0 ± 2.2)	10.61 (10.85 ± 0.59)
50	1.11 (1.11 ± 0.01)	15.01 (14.89 ± 0.23)	69.2 (66.2 ± 2.8)	11.53 (10.85 ± 0.59)
55	1.12 (1.11 ± 0.02)	15.13 (15.05 ± 0.13)	67.3 (66.9 ± 1.7)	11.40 (11.16 ± 0.16)
60	1.09 (1.10 ± 0.01)	15.25 (14.83 ± 0.28)	69.5 (67.3 ± 2.4)	11.55 (10.99 ± 0.37)
65	1.09 (1.09 ± 0.02)	14.76 (14.78 ± 0.35)	68.4 (66.1 ± 2.3)	11.00 (10.69 ± 0.36)
70	1.11 (1.10 ± 0.01)	14.53 (14.76 ± 0.28)	66.1 (63.7 ± 2.3)	10.66 (10.45 ± 0.53)
75	1.11 (1.09 ± 0.01)	14.89 (14.87 ± 0.11)	62.4 (63.7 ± 2.3)	10.31 (10.31 ± 0.25)

[a]The best values are given, followed by the averages and standard derivations in parentheses, calculated from at least eight devices.

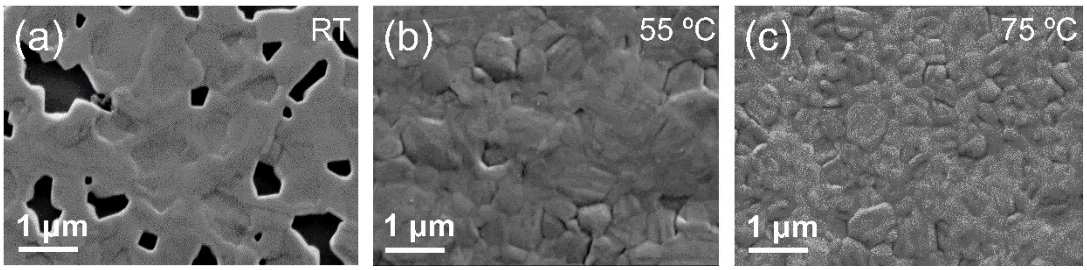

Fig. S11 Top-view SEM images of (a) RT-casting and (b,c) hot-casing processed $CsPbI_2Br$ films with substrate temperatures of (b) 55 °C and (c) 75 °C. All the samples underwent post-annealing at 340 °C for 10 min.

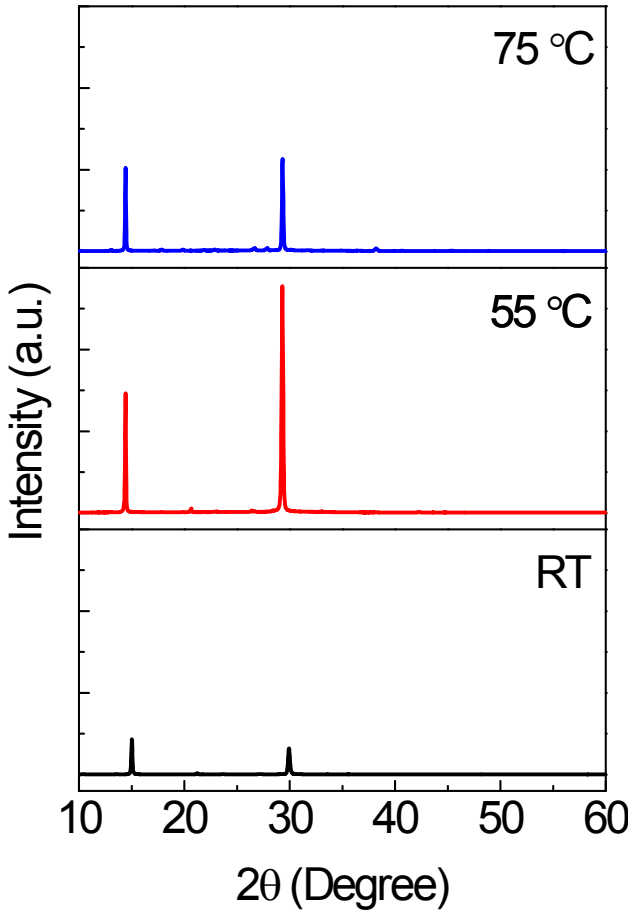

Fig. S12 XRD patterns of RT-casting and hot-casting processed $CsPbI_2Br$ films with substrate temperatures of 55 °C and 75 °C. All the samples underwent post-annealing at 340 °C for 10 min.

9. Optimization of post-annealing temperatures

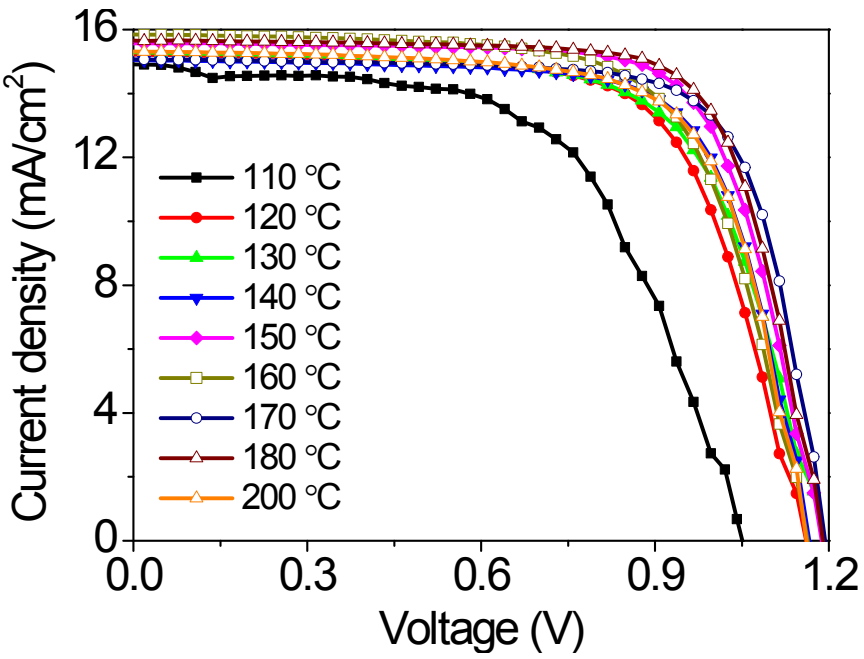

Fig. S13 *J-V* characteristics of $CsPbI_2Br$-based PSCs fabricated by hot-casting method with subsequent post-annealing at different temperatures. The substrate temperature was kept at 55 °C.

Table S3. Photovoltaic performance of the $CsPbI_2Br$-based PSCs fabricated by hot-casting method with subsequent post-annealing at different temperatures. The substrate temperature was kept at 55 °C.

Substrate temp. (°C)	V_{oc}[a] (V)	J_{sc}[a] (mA cm^{-2})	FF[a] (%)	PCE[a] (%)
100	No Efficiency			
110	1.04 (1.01 ± 0.04)	15.21 (14.64 ± 0.45)	62.8 (56.8 ± 4.4)	9.93 (8.56 ± 1.10)
120	1.17 (1.12 ± 0.03)	15.04 (14.88 ± 0.59)	71.0 (69.4 ± 1.8)	12.45 (11.60 ± 0.71)
130	1.16 (1.15 ± 0.01)	15.21 (15.24 ± 0.44)	67.9 (67.2 ± 3.1)	11.98 (11.79 ± 0.36)
140	1.16 (1.18 ± 0.01)	15.04 (15.14 ± 0.39)	72.2 (69.2 ± 1.9)	12.58 (12.33 ± 0.15)
150	1.19 (1.18 ± 0.01)	15.58 (15.67 ± 0.10)	70.0 (69.9 ± 2.0)	13.35 (12.97 ± 0.33)
160	1.16 (1.18 ± 0.01)	15.85 (15.55 ± 0.22)	68.3 (66.3 ± 1.7)	12.56 (12.13 ± 0.35)
170	1.19 (1.18 ± 0.01)	15.07 (15.07 ± 0.08)	74.1 (71.6 ± 1.5)	13.29 (12.79 ± 0.34)
180	1.19 (1.17 ± 0.02)	15.66 (15.58 ± 0.15)	74.1 (72.4 ± 1.4)	13.80 (13.23 ± 0.56)
200	1.16 (1.15 ± 0.01)	15.32 (15.28 ± 0.08)	70.0 (69.6 ± 2.2)	12.34 (12.20 ± 0.24)

[a]The best values are given, followed by the averages and standard derivations in parentheses, calculated from at least eight devices.

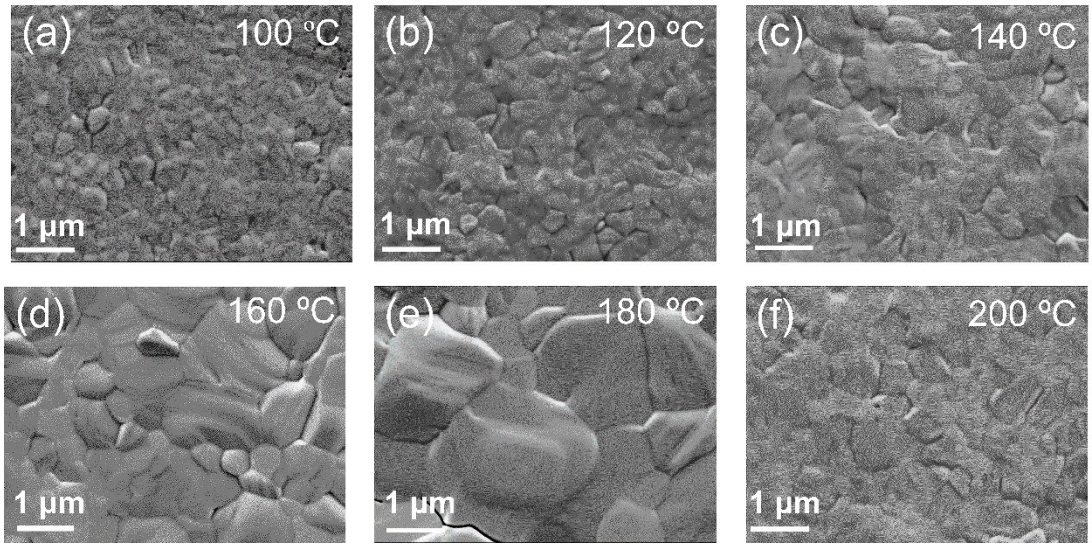

Fig. S14 Top-view SEM images of hot-casting processed $CsPbI_2Br$ films with subsequent post-annealing at (a)100 °C, (b) 120 °C, (c) 140 °C, (d) 160 °C, (e) 180 °C and (f) 200 °C. The substrate temperature was kept at 55 °C.

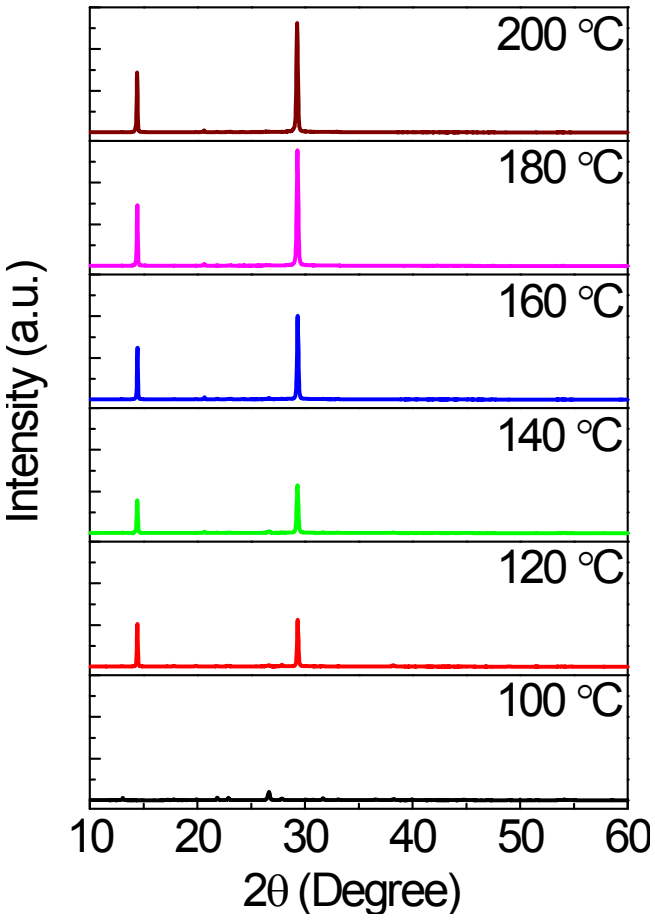

Fig. S15 XRD patterns of hot-casting processed $CsPbI_2Br$ films with subsequent post-annealing at (a)100 °C, (b) 120 °C, (c) 140 °C, (d) 160 °C, (e) 180 °C and (f) 200 °C. The substrate temperature was kept at 55 °C.

10. *J-V* curves measured under different scan rates

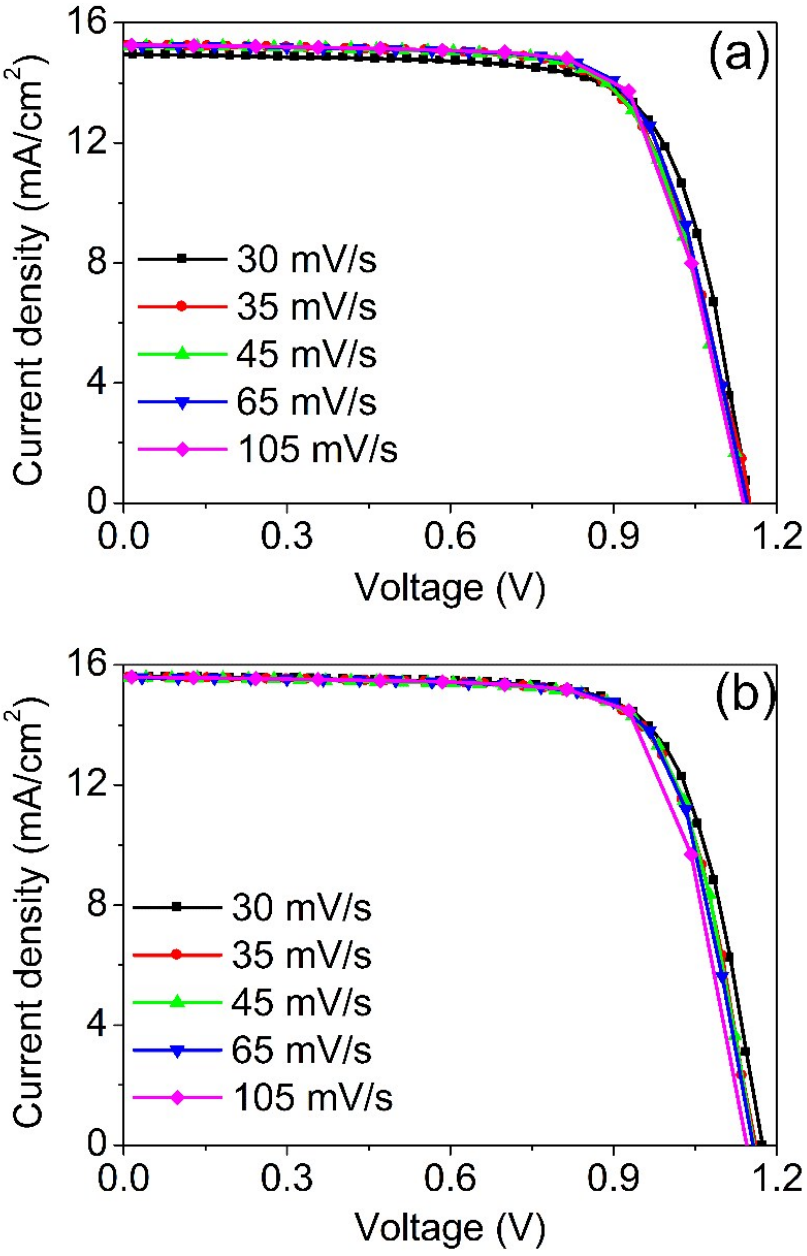

Fig. S16 *J-V* characteristics, measured under different scan rates, of $CsPbI_2Br$-based PSCs fabricated by hot-casting method (substrate temperature was kept at 55 °C) with subsequent post-annealing at (a) 120 °C and (b) 180 °C.

11. *J-V* curves measured under different scan directions

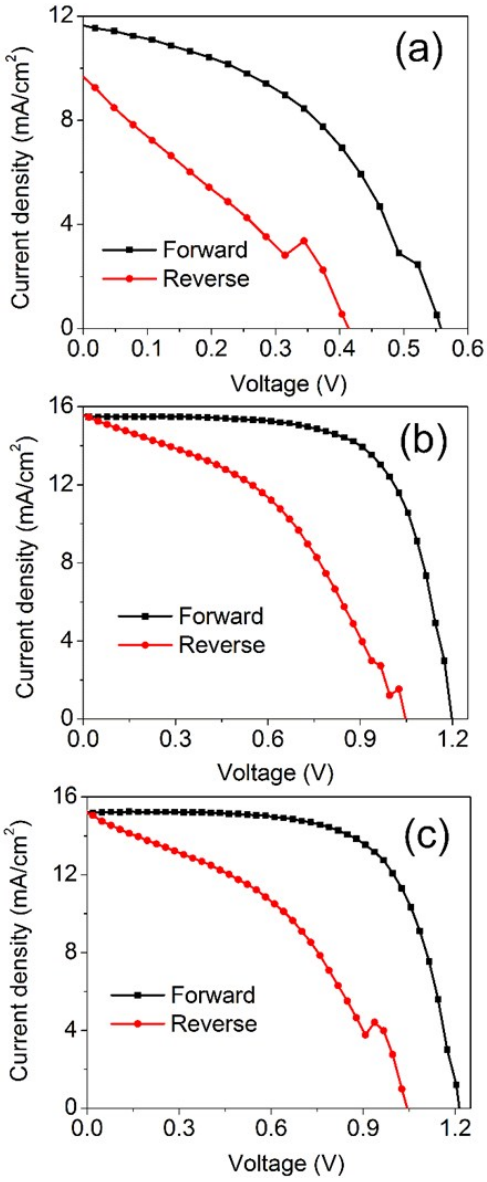

Fig. S17 *J-V* curves, measured in the forward and reverse scan directions, of the $CsPbI_2Br$-based PSCs fabricated by (a) conventional RT-casting method and (b,c) hot-casting method (substrate temperature was kept at 55 °C) with subsequent post-annealing at (b) 180 °C and (c) 120 °C for the perovskite films.

12. Thermal stability tests of $CsPbI_2Br$ and $CH_3NH_3PbI_3$ PSCs

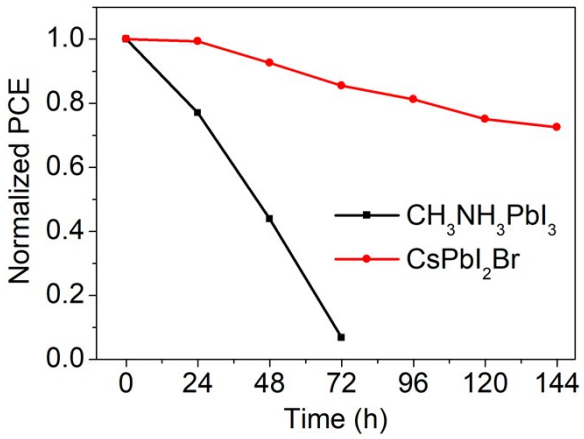

Fig. S18 Long-term PCE stability of the PSCs based on hot-casting processed $CsPbI_2Br$ and traditional organic-inorganic hybrid perovskite $CH_3NH_3PbI_3$, which were placed on a hot plate at 100 °C in a N_2-filled glove box with H_2O and O_2 levels below 1 ppm. The device structure of $CH_3NH_3PbI_3$ PSCs is similar to that of $CsPbI_2Br$ PSCs, and the $CH_3NH_3PbI_3$ perovskite layer was made by one-step anti-solvent method.

13. References

1 Z. J. Shi, J. Guo, Y. H. Chen, Q. Li, Y. F. Pan, H. J. Zhang, Y. D. Xia and W. Huang, *Adv. Mater.*, 2017, **29**, 1605005.

2 W. S. Yang, B. W. Park, E. H. Jung, N. J. Jeon, Y. C. Kim, D. U. Lee, S. S. Shin, J. Seo, E. K. Kim, J. H. Noh and S. I. Seok, *Science*, 2017, **356**, 1376-1379.

3 D. Bai, H. Bian, Z. Jin, H. Wang, L. Meng, Q. Wang and S. Liu, *Nano Energy*, 2018, **52**, 408-415.

4 A. Dualeh, N. Tétreault, T. Moehl, P. Gao, M. K. Nazeeruddin and M. Grätzel, *Adv. Funct. Mater.*, 2014, **24**, 3250-3258.

5 T. Su, X. Li, Y. Zhang, F. Zhang and Z. Sheng, *Phys. Chem. Chem. Phys.*, 2017, **19**, 13147-13152.